JMEPEG (1998) 7:407-419

The Effect of Segregation on the Austemper Transformation and Toughness of Ductile Irons

B.Y. Lin, E.T. Chen, and T.S. Lei

(Submitted 19 December 1994; in revised form 5 November 1997)

The effect of segregation of alloying elements on the phase transformation of ductile iron during austempering was investigated. Four heats, each containing 0.4%Mn, 1%Cu, 1.5%Ni, or 0.4%Mo (wt%) separately, were melted; then three different sizes of casting bars (3, 15, and 75 mm diameter) were poured from each heat. The distribution and the degree of segregation of certain elements were quantitatively analyzed using an electron microprobe. A personal computer (PC)-controlled heat treating system was used to measure electrical resistivity, and the information on resistivity variations was used to analyze the effect of segregation on phase transformations during austempering. Also, Charpy impact and Rockwell hardness tests were performed to determine the effect of segregation on properties.

Results of the electron microprobe analysis showed that the degree of segregation of alloy elements increases with an increase in diameter of the casting bars (i.e., an increase of solidification time of castings). The degree of segregation of alloy elements, represented by segregation ratio (SR) (the maximum concentration of element in cell divided by the minimum concentration of element in cell), varied linearly with the casting modulus (*M*) (volume of casting divided by surface area of casting). Regarding the segregating tendency among alloy elements, positive segregating elements Mn and Mo showed more segregation than the negative segregating elements Si, Cu, and Ni. In addition, segregation of Mo was more significant than Mn, and that for Cu was greater than Ni and Si.

Between the time of finishing the first stage and beginning the second stage of bainite reaction in ductile irons, there is a significant "processing window," Δt_i, for austempering to obtain optimum mechanical properties. From the electrical resistivity data, it was observed that the austempering temperature plays a major role in the processing window. There was a narrow window at 400 °C but a larger one at 350 °C. Additionally, the microsegregation of alloying elements led to variation of the time of phase transformation for various regions in the grain cells of ductile iron which caused the processing window to decrease. The span of the processing window decreased with an increase in degree of segregation.

There was no significant difference in the hardness of the alloys in various diameter specimens. However, the impact toughness was significantly affected by the segregation. The impact values in 15 mm specimens with less degree of segregation were greater than those in 75 mm specimens with significant segregation.

The Ni, Cu, and Mn alloys that were austempered to complete the first stage of bainite formation had approximately the same impact values for all diameter samples. The Mo alloy upon austempering produced no bainite, but it had much untransformed retained austenite in the intercellular regions and, therefore, had lower impact values.

Keywords	austempering, ductile iron, heat treating, segregation, toughness

1. Introduction

With proper austempering treatment, ductile cast iron, having excellent mechanical properties, can have those properties improved. The austempering heat treatment for ductile cast iron is similar to that for steel. The cast iron must be held for a sufficient period of time, first at the austenitizing temperature, to allow the matrix of ductile iron to be austenitized completely, followed by quenching to 300 to 400 °C. The cooling rate must be sufficient to prevent austenite from transforming into proeutectoid ferrite or pearlite. Finally, the ductile iron is held isothermally at that temperature for a proper length of time. During the process of isothermal holding, the following two stages of bainite reaction occur. In the first stage, the remaining austenite retained after the high temperature quench decomposes into ferrite and carbon-rich austenite. In the second stage, the high-carbon austenite eventually decomposes to ferrite and carbide. After completion of the first stage, the microstructure of the matrix in austempered ductile iron (ADI) contains acicular ferrite and carbon-rich austenite, giving ADI an outstanding mechanical property of high strength and good ductility. If the isothermal holding time is long enough to permit the reaction to continue to the second stage, the carbon-rich austenite decomposes to ferrite and carbide. Since the carbon-rich austenite is continuously being eliminated, carbide particles constantly form film on interfaces which provide relatively convenient crack paths, and ductility decreases. Therefore, the isothermal

B.Y. Lin, E.T. Chen, and **T.S. Lei,** Department of Mechanical Engineering and Technology, National Taiwan Institute of Technology, Taipei, Taiwan 10722, Republic of China.

holding time should be limited to the completion of the first stage, and the reaction of the second stage should be avoided (Ref 1-6).

Many kinds of experimental techniques, such as quantitative metallography (Ref 7, 8), magnetic change (Ref 9), dilatometry (Ref 9, 10), x-ray diffraction (XRD) (Ref 11, 12), and electrical resistivity change (Ref 13), may be used to measure the phase transformation during the austempering of ductile irons. However, by measuring the electrical resistivity, the time to start and to finish for both stages of reaction can be determined (Ref 13, 14). Figure 1 illustrates the variation of resistance and volume fraction austenite with austempering time for a ductile iron austempered at 400 °C (Ref 14). The resistance curve has three plateaus. In the first plateau, the ductile iron matrix is supercooled austenite before entering the reaction of the first stage, so the resistance is constant. Once the bainite begins to form in the first stage, the curve shows the first decrease. When the first stage is completed, most of the matrix should be acicular ferrite and carbon-rich austenite, which remains during the second plateau. Once the reaction enters the second stage, the curve again decreases and then exhibits the third plateau upon completing the reaction of the second stage, during which the structure of ADI becomes stabilized ferrite and carbide. The first reaction plateau is reached at approximately 700s, which is the time the reaction of the first stage is completed. After 10 000s, the curve once again exhibits a significant drop, indicating the start of the second stage.

The amount of retained austenite present after cooling to 25 °C depends on the carbon content of the austenite, which is greater when the carbon content is higher. In austempering, during the first stage bainite formation, the amount of bainite increases, but since the carbon content of the remaining austenite also increases, then the amount of retained austenite after cooling to 25 °C increases. In the second stage of bainite formation, the amount of bainite increases, and the level of retained austenite after quenching decreases. Thus the time between the end of the first and the beginning of the second stage produces the maximum amount of retained austenite. This processing window Δt_i is used in ADI to produce the optimal mechanical properties (Ref 15-17).

For the successful manufacture of ADI, proper selection and strict control of the austenitizing temperature, quenching rate, austempering temperature, and isothermal holding time are required (Ref 18).

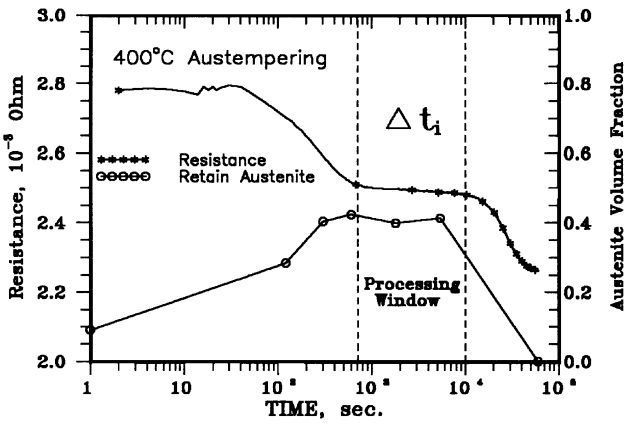

Fig. 1 Variation of electrical resistance and volume fraction austenite with austempering holding time for ductile iron (Ref 14)

For ADI, particularly in heavy section castings, alloying elements are frequently added to increase the hardenability to avoid ferrite or pearlite forming from austenite during quenching and to enhance the austemperability in the process of isothermal treatment. However, it has been shown by a number of studies that positively segregating elements, such as Cr, Mn, Mo, and V, tend to segregate at the end of solidification to the cell boundary region, while those negative segregating elements, such as Si, Cu, and Ni, are apt to segregate in the early part of solidification or around the nodular graphite during the solidification of heavy section ductile iron (Ref 19-22). Microsegregation of alloying elements during solidification can cause defects, namely carbides and porosity, in the as-cast microstructure and can result in different hardenability and phase transformation rates among the matrix of austenite cells during austempering, which increases the difficulty in controlling the austempering heat treatment and strongly affects the mechanical properties of ADI (Ref 23-25).

The effect of microsegregation on the phase transformation during austempering and on the mechanical properties of ADI was investigated. First, castings containing Mn, Cu, Ni, and Mo separately were made, and the distribution of each element was measured quantitatively using the electron microprobe for determination of the degree of segregation. Then a special vacuum heat treating system was used to measure the electrical resistance during austempering, and these results were used to investigate the effect of microsegregation of alloy elements upon the austempering transformation. Finally, impact and hardness tests were performed to compare the toughness and hardness.

2. Experimental Procedure

Four different compositions of ductile iron heats containing, individually, 0.4% Mn, 0.4%Mo, 1%Cu, and 1.5% Ni (wt%) were made. For accurate control of the composition in each heat, master ingots were prepared in a high frequency induction melting furnace using a charge composed of pig iron, steel scrap, ferrosilicon, and carbon. For the melting process of those heats containing Mn, Ni, or Cu, a 20 kg piece of a master ingot was melted in the furnace; then ferromanganese, electrolytic nickel, or pure copper was added. The melt was heated up to around 1530 °C; then the melt was treated using the sandwich technique and poured at approximately 1430 °C into a mold. To melt the Mo completely, the process of the heat containing Mo was made differently. To a 20 kg master ingot, ferromolybdenum particles approximately 1 mm in diameter were placed in the melting furnace; then the melt was heated two times up to 1750 °C and held for 30 min. After the temperature was lowered to ~1530 °C, the melt was poured into a ladle and treated by the sandwich technique. It was then cast at ~1430 °C into a mold.

For each heat, 12 pieces each 3 mm diameter and 100 mm long, 6 pieces each 15 mm diameter and 150 mm long, and one piece 75 mm diameter and 150 mm long were cast. A graphite mold preheated to 900 °C was used for casting the 3 mm diameter bars, and a CO_2 mold was used for the 15 and 75 mm diameter bars.

Specimens taken at the center part of the casting bars, shown in Fig. 2, were austenitized in air at 900 °C for 1 h and quenched in water to allow the distribution of alloying elements in the matrix to be similar to that occurring after austenitizing in austempering heat treatment process. The specimens were first studied using an optical microscope. The nodularity, nodule counts, and nodule mean diameter of specimens were then examined with Quantiment 520 image analysis system (Cambridge Instruments). The quantitative measurement of the distribution of alloying elements was made using a JEOL Superprobe 733 electron microprobe (EPMA) with operating conditions of: 25 kV acceleration voltage; 2.5×10^{-3} A beam current; 40° take-off angle; and 1 μm beam diameter. Finally, the deviations from the results of EPMA were checked and amended with the results of spectroscopic analysis in the chill test piece.

To select the regions for quantitative measurement in each specimen, more than three pairs of graphite nodules abutted to one another with the diameter of each nodule close to the mean diameter were chosen. The positions for measuring by EPMA between two nodules were provided for those five points between two graphite nodules, encompassing the edge of the module (Zone I), the major portion of the matrix (Zone II), and the cell boundary (Zone III) as indicated in Fig. 3.

The apparatus used to determine the electrical resistivity is shown schematically in Fig. 4. The sample, in the form of a rod (typically 100 mm long and 3 mm diameter), is self heated by current from a programmable direct current power supply. On the sample are welded two small diameter wires about 8 mm apart, and the voltage across the two wires is measured. Also the voltage drop across a standard resistor in series with the sample is measured to obtain the current through the sample. The product of these measurements gives the resistance of the sample. The sample temperature is monitored by two small diameter K-type thermocouples welded to it. The voltage and thermocouple signals are amplified, then processed and stored by a PC. The PC was interfaced with the programmable power supply, and this allowed the computer program to produce a preset temperature-time process for the sample. Thus samples were heated to the austenitizing temperature at a preset rate, held for one hour at 900 °C, cooled with a spray of liquid nitrogen to a preset austempering temperature of 350 or 400 °C, then held at this temperature for the desired time. The heat treatment process is carried out in vacuum. The hardware and software of this system were shown in greater detail in a recent report (Ref 14).

The specimens for the resistance measurements were ~3 mm diameter and ~100 mm long. Therefore, bars that were 3 mm diameter and 100 mm long cast from four heats were used directly without being further machined. Cast bars 15 mm diameter were roughly machined to rods about 3.5 mm diameter and 100 mm long, then they were centerless ground to specimens 3 mm diameter. For the 75 mm diameter rods, $15 \times 15 \times 150$ mm bars were taken from the part as shown in No. 2, Fig. 2. They were then turned into rough rods each ~3.5 mm diameter, and finally they were cut and ground into specimens of 3 mm diameter and 100 mm long.

Unnotched Charpy impact specimens $10 \times 10 \times 15$ mm were made from the 15 mm diameter cast bars and the 75 mm cast bars as indicated in No. 2, Fig. 2. Three conditions (as-cast, 400 °C, and 350 °C austempering) for the specimens were selected, and impact tests were performed in a Tinius Olsen Charpy impact tester (Tinius Olsen Testing Machine Co., Willow Grove, PA) at 25 °C. Austempering for impact specimens was performed in salt baths. Heat treatment condition involved austenitization at 900 °C for 1 h and austempering at 400 °C for 50 min and 350 °C for 5 h. These austempering holding times

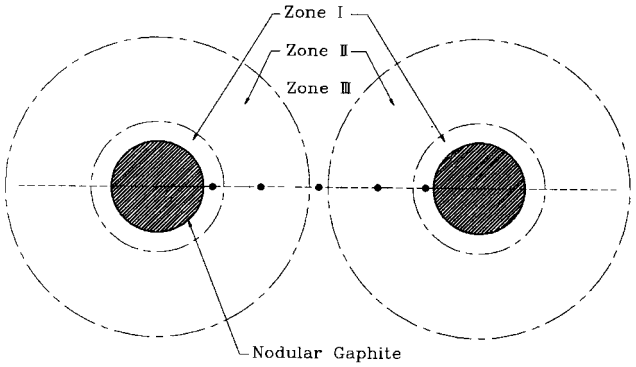

Fig. 3 Schematic of the positions indicated by point for quantitative EPMA measurement in Zones I, II, and III between two nodules

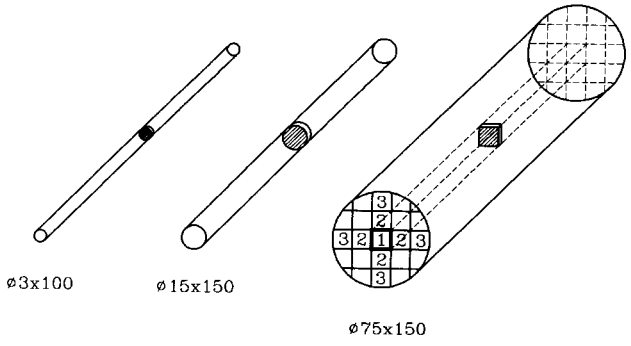

Fig. 2 Schematic of 3 mm, 15 mm, and 75 mm size casting bars. Sections in each bar for EPMA measurement. The parts of No. 2 in 75 mm bar for electrical resistivity measurement and impact test

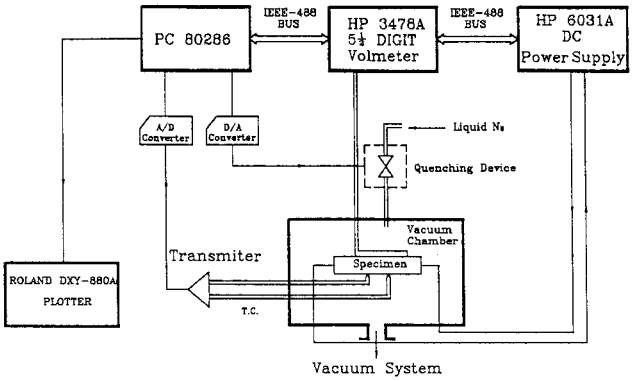

Fig. 4 Block diagram illustrating the personal computer controlled vacuum heat treating system

were determined from the processing window based on each electrical resistivity record. After impact testing, Rockwell hardness readings were taken on each side of the impact specimens, and the values were averaged. Specimens for metallographic examination were cut from impact specimens, mounted, ground, polished, and etched with 3% nital. Specimens were examined by an optical microscope.

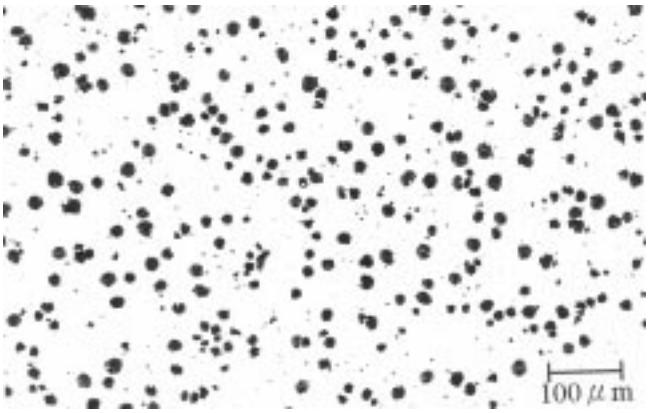

(a)

(b)

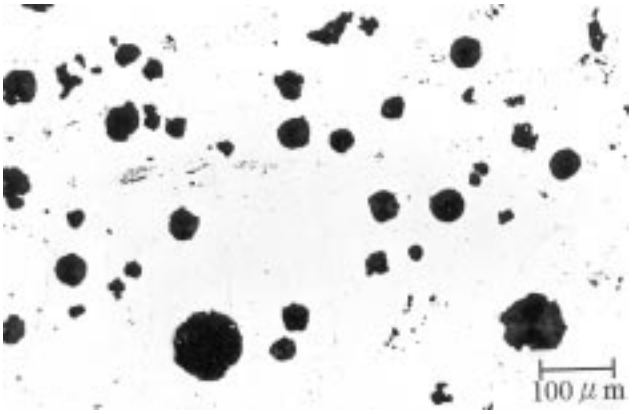

(c)

Fig. 5 Microstructures of quenched sample DI-22 after austenitizing at 900 °C for 1 h. Unetched. (a) 3 mm specimen. (b) 15 mm specimen. (c) 75 mm specimen

3. Results and Discussion

3.1 Microsegregation of Alloying Elements

The chemical analyses of the heat in this experiment are presented in Table 1. Table 2 lists the average value of nodularity, nodule counts, and nodular mean diameter obtained using the Quantimet 520 image analysis system on quenched specimens. Figure 5 shows the microstructures of unetched DI-22 specimens. Comparison of Table 2 with Fig. 5 shows that the nodularity of each specimen is over 85%; nodule counts and nodular mean diameters of those specimens in the same diameter but with different heat are very close to one another. However, a significant difference is observed among specimens with different diameters, most likely due to the distinctly different nucleation and growth rates during solidification among the casting bars. The nodule count of 3 mm specimens is greater than 400 N/mm^2 with mean nodular diameter of ~14 μm. In 15 mm specimens, it is ~250 to 300 N/mm^2, with mean nodular diameter of ~21 μm; in 75 mm specimens, it is ~100 N/mm^2, with 36 μm mean nodular diameter.

The compositions of the alloying elements quantitatively measured by EPMA at the solidification cell boundaries (Zone III), the area along nodular graphite (Zone I), and the major portion of the matrix (Zone II) are listed in Table 3. Each of the data for Zones I and II in Table 3 is the mean value of more than six readings. For Zone III, it is for more then three readings. Data for Si and Mn were measured in DI-33 specimens. The average composition of Si is 2.46%, and the average composition of Mn is 0.47%. For Ni in DI-22 specimens, it is 1.36%. For Cu in DI-23 specimens, it is 0.86%, and for Mo in DI-71 specimens, it is 0.35%.

The degree of alloy segregation is represented by segregation ratio, defined as:

$$SR = \frac{C_{max}}{C_{min}} \qquad \text{(Eq 1)}$$

where C_{max} is the maximum composition of the alloy element in the cell and C_{min} is the minimum composition of the alloy

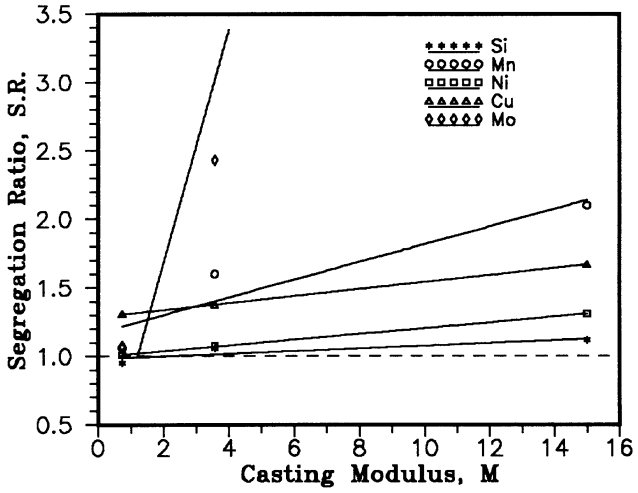

Fig. 6 Variation of the segregation ratio with the casting modulus

element in the cell. The segregation ratios are listed in Table 3. For those specimens containing Mn and Mo, the values of SR are the values in Zone III divided by the values in Zone I; for Si, Cu, and Ni, values in Zone I are divided by the values in Zone III. According to the Chvorinov rule (Ref 26)

$$t_f = C\left[\frac{V}{A}\right]^2 \quad \text{(Eq 2)}$$

where t_f is the solidification time for a casting, V is the volume of a casting, A is the surface area of a casting related to heat transfer, and C is a constant related to the mold. The solidification time t_f for the casting is in proportion to the square of the ratio of volume to surface area V/A. If the ratio V/A is defined as the casting modulus M, then

$$t_f = CM^2 \text{ and } M \propto \sqrt{t_f}$$

The casting modulus M for the 3×100, 15×150, and 75×150 mm specimens is 0.74, 3.57, and 15 mm, respectively. Figure 6 plots the segregation ratio for elements in Table 3 with the casting modulus M of specimens of various diameters. The segregation ratio for each alloying element changes almost proportionally with the increase of modulus (i.e., the increase of the square root of the solidification time required for casting). Comparison of the segregating tendency of each element in the cell indicates that all positive segregation elements are more significant than negative segregation elements. Among all negative segregation elements, the significant segregation tendency of Cu is greater than that of Ni and Si; whereas among those positive segregation elements, the segregation tendency of Mo is more significant than that of Mn.

Upon decreasing the cooling rate during solidification, the austenite dendrite cell size increases; hence the distance for homogenization during subsequent cooling is increased. This leads to more segregation for less rapid solidification. Thus the distribution of the alloying elements will be relatively far removed from the average concentration (more segregated), and the distribution of the alloying elements can be described by the Scheil equation. Furthermore, the solidification process of ductile iron can be modeled as spherical growth, and it has been established that the alloy element distribution is a function of the cube of the growing cell radius (Ref 27).

Table 1 Chemical composition of heats

Heat No.	Composition, wt%								
	C	Si	Mn	P	S	Mg	Mo	Ni	Cu
DI-22	3.68	2.52	0.29	0.033	0.009	0.023	…	1.36	…
DI-23	3.56	2.46	0.24	0.031	0.011	0.028	…	…	0.86
DI-33	3.73	2.46	0.47	0.031	0.010	0.037	…	…	…
DI-71	3.53	2.53	0.25	0.039	0.015	0.031	0.35	…	…

3.2 Segregation Impact on Austempering Reaction

Figure 7 shows schematically an isothermal heat treatment made at an austempering temperature and the electrical resistivity curve recorded during the isothermal holding time. The

Table 2 Nodularity data of specimens studied

Sample No.	Diameter, mm	Nodularity, %	Nodules, No./mm²	Mean diameter of nodules, μm
DI-22	3	86	580	16
	15	85	287	21
	75	82	90	38
DI-23	3	85	401	18
	15	86	275	23
	75	88	100	34
DI-33	3	77	670	13
	15	87	314	21
	75	88	90	35
DI-71	3	81	847	12
	15	80	253	20
	75	84	97	35

Data average of 5 readings

Table 3 Electron microprobe results and the segregation ratio of specimens studied

Alloying element	Sample No.	Diameter, mm	Zone I(a), wt%	Zone II(a), wt%	Zone III(b), wt%	Segregation ratio SR(c)
Si	DI-33	3	2.42	2.54	2.55	0.95
		15	2.55	2.53	2.41	1.06
		75	2.55	2.60	2.28	1.12
Mn	DI-33	3	0.45	0.52	0.48	1.06
		15	0.34	0.46	0.55	1.61
		75	0.38	0.40	0.82	2.14
Ni	DI-22	3	1.35	1.37	1.34	1.01
		15	1.48	1.46	1.38	1.08
		75	1.51	1.42	1.15	1.31
Cu	DI-23	3	0.95	0.74	0.72	1.31
		15	1.01	0.95	0.74	1.37
		75	0.98	0.84	0.59	1.67
Mo	DI-71	3	0.34	0.33	0.36	1.07
		15	0.14	0.16	0.34	2.43
		75	0.07	0.13	0.94	12.93

(a) Compositions are average of more than 6 data. (b) Compositions are average of more than 3 data. (c) For Mn and Mo, SR is Zone III divided by Zone I. For Si, Ni, and Cu, SR is Zone I divided by Zone III.

IT diagram of the homogeneous matrix of ductile iron within the temperature scope of bainite transformation can be explained by two pairs of solid reaction lines. One pair is $B1_s$ and $B1_f$ illustrating the start and finish time of the first-stage reaction, the other pair is $B2_s$ and $B2_f$ representing the beginning and completion of the second-stage reaction, as shown in Fig. 7(a). If the segregation of alloying elements existing in the grain cell leads to the difference of the time of phase transformation for various regions of the cell, some portions will delay the bainite reaction, and some will advance the time of reaction, as shown by the dashed and dotted curves in Fig. 7(a). Figure 7(b) shows the electrical resistance records influenced by the segregation of alloying elements. The microsegregation in ductile iron will cause the processing window Δt_i to decrease.

Figures 8 and 9 show the electrical resistance for Ni (DI-22), Cu (DI-23), Mn (DI-33), and Mo (DI-71) alloys in different diameters with austempering holding time at 350 °C and 400 °C. In the figures for austempering at 400 °C (Fig. 9), the curves of resistivity completely record both the first and the second stages of bainite reaction; whereas at 350 °C (Fig. 8), the curves stop at the beginning of the second stage. The reason the austempering process at 350 °C for this experiment discontinues upon entering the second stage is that the completion of the reaction of the second stage at 350 °C austempering requires a very long time.

The changes of the electrical resistivity curves during the austempering at 350 °C are shown in Fig.8(a) through (d). It is clearly seen that the specimen diameter (i.e., the various degree of segregation) significantly affects the processing window. The curve of 3 mm specimens in each figure has the widest processing window, while that of the 75 mm specimen has the narrowest. The span of the processing window is reduced with an increase in the degree of segregation. Similar changes occur in the electrical resistivity curves during 400 °C austempering (Fig. 9). The curve within the processing window for 3 mm specimen in each figure is flattened and has a wide span. For 15 mm specimens, the curve starts to incline as the span of the processing window decreases. For 75 mm specimens, the inclination of the curve becomes larger while its processing window span is difficult to identify. The decrease of the resistivity curve within the processing window is attributed to the segregation of alloy elements in the grain cells and to a very high rate of bainite transformation. Segregation causes local differences in the reaction time for the bainite formation. Segregation also produces a decrease in the resistivity within the desired processing window.

The completion times of the first decrease in resistivity in Fig. 8 and 9 are defined as completing the first stage of bainite reaction, while those of the second decrease are defined as starting the second stage. Table 4 lists the times of finishing the first stage and starting the second stage of bainite transformation of all curves in Fig. 8 and 9. Figure 10 presents the partial isothermal transformation diagram within the range of 350 to 400 °C drawn using the data in Table 4, wherein the area between the $B1_f$ and $B2_s$ lines should be the significant window of time Δt_i for ductile irons austempered at 350 to 400 °C. From Fig. 10, a narrow processing window, falling within approximately 10^3 to 5×10^3 seconds, is found at 400 °C for various alloys in different diameter specimens, and a wider window, approximately 2×10^3 to 10^5 seconds, at 350 °C. Obviously, the austempering temperature is the most critical factor affecting the span of the processing window.

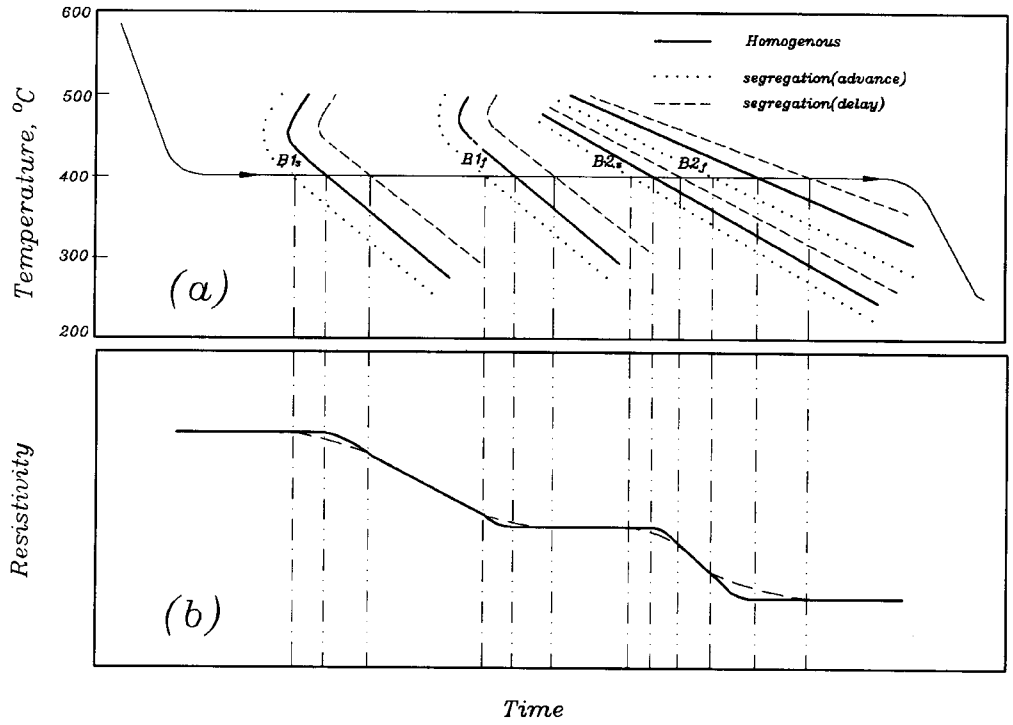

Fig. 7 (a) Schematic representation of a partial IT diagram of a homogeneous matrix ductile iron (solid lines), showing the effect of microsegregation (dashed and dotted lines) within the bainite transformation scope. (b) Influence of the segregation on the electrical resistivity of ductile irons during austempering

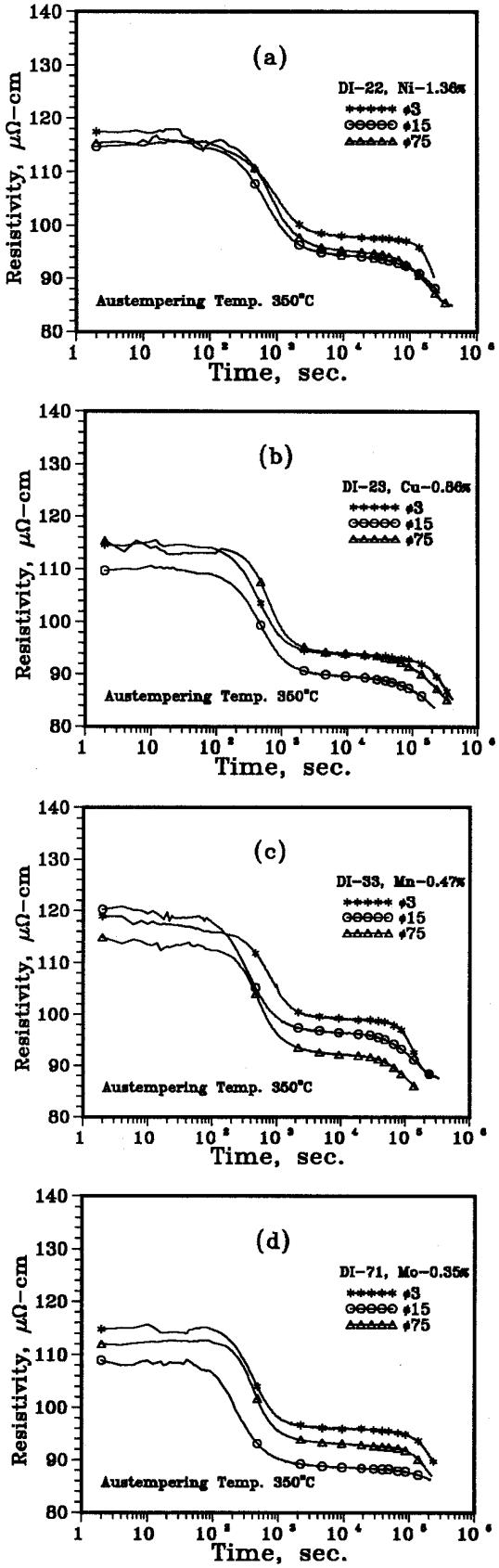

Fig. 8 Electrical resistivity record of each alloy in various diameters austempered at 350 °C: (a) Ni alloy (DI-22). (b) Cu alloy (DI-23). (c) Mn alloy (DI-33). (d) Mo alloy (DI-71)

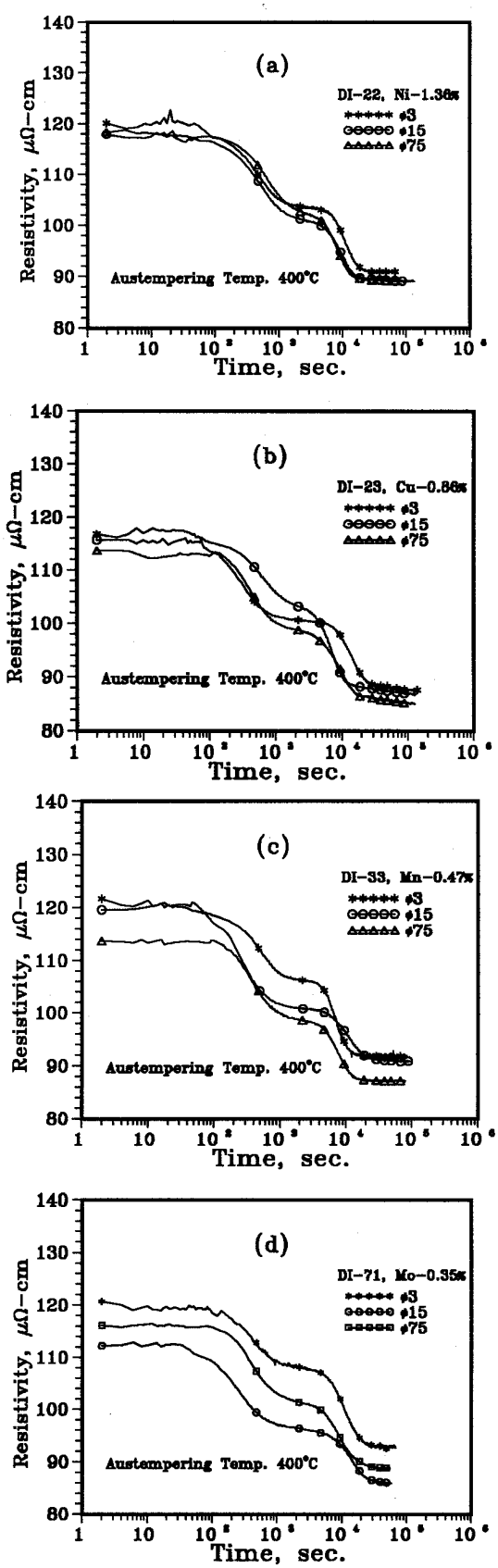

Fig. 9 Electrical resistivity record of each alloy in various diameters austempered at 400 °C: (a) Ni alloy (DI-22). (b) Cu alloy (DI-23). (c) Mn alloy (DI-33). (d) Mo alloy (DI-71)

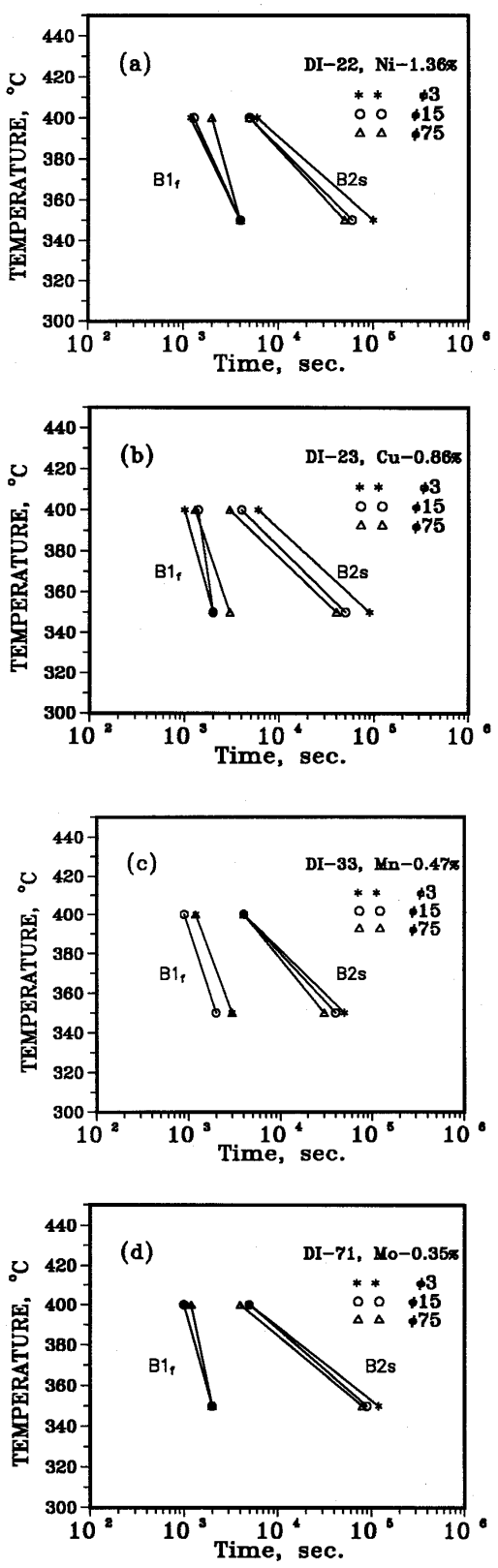

Fig. 10 Partial IT diagrams of each alloy in various diameter, including $B1_f$ (finishing the first stage of bainite reaction) and $B2_S$ (starting the second stage of bainite reaction). (a) Ni alloy (DI-22). (b) Cu alloy (DI-23). (c) Mn alloy (DI-33). (d) Mo alloy (DI-71)

As for the influence of the specimen diameter (i.e., the different degree of segregation) on the span of the processing window in the IT diagram, Fig. 10 shows that an increase of the diameter leads to narrowing of the processing window. The span of the processing window between 400 to 350 °C for the Ni alloy as shown in Fig. 10(a) is slightly wider for the 3 mm specimen than the 15 mm specimen, while the span for 75 mm is significantly narrow. There is a definite effect of specimen diameter upon the processing window for Cu alloys as illustrated in Fig. 10(b). Within 400 to 350 °C, the processing window for 3 mm specimens is wide, followed by that of 15 mm specimens. That of 75 mm is much smaller. This is possibly caused by the tendency of segregation for Cu being greater than for Ni. For the Mn alloy, Fig. 10(c), the impact upon the span of processing window at 400 °C is less significant, but at 350 °C, the span of processing window is also reduced as the diameter of the specimen increases. Figure 10(d) illustrates the IT diagram of Mo alloys. The 3 mm casting rod with the least segregation is found with the widest span of processing window within the range of 400 to 350 °C, and the processing window is reduced for both 15 mm and 75 mm specimens due to segregation of Mo in the matrix of these two specimens.

Table 4 The finish time of first stage and start time of second stage of bainite formation of all curves in Fig. 8

Sample No.	Diameter, mm	Time, s			
		$B1_f$		$B2_s$	
		400 °C	350 °C	400 °C	350 °C
DI-22 (Ni)	3	1200	4000	6000	100 000
	15	1300	4000	5000	60 000
	75	2000	4000	5000	50 000
DI-23 (Cu)	3	1000	2000	6000	90 000
	15	1400	2000	4000	50 000
	75	1300	3000	3000	40 000
DI-33 (Mn)	3	1200	3000	4000	50 000
	15	900	2000	4000	40 000
	75	1200	3000	4000	30 000
DI-71 (Mo)	3	1000	2000	5000	120 000
	15	1000	2000	5000	90 000
	75	1200	2000	4000	80 000

Table 5 Mechanical properties of specimens from 15 mm and 75 mm cast bars

Sample No.	Diameter, mm	Impact energy (a), kg-m			Hardness (HRC)(b)		
		Austempering			Austempering		
		400 °C	350 °C	As-cast	400 °C	350 °C	As-cast
DI-22 (Ni)	15	14.4	14.9	4.8	32.2	34.7	28.4
	75	9.9	10.1	3.7	28.6	32.2	16.9
DI-23 (Cu)	15	15.5	13.5	4.5	32.3	37.0	31.6
	75	11.8	9.7	2.0	32.6	38.0	23.6
DI-33 (Mn)	15	15.7	12.8	5.1	31.5	34.9	21.7
	75	9.6	9.0	5.5	29.7	32.9	10.5
DI-71 (Mo)	15	12.0	10.0	5.3	33.3	40.1	22.9
	75	5.7	7.4	4.3	31.8	35.7	8.1

(a) Average of 3 readings. (b) Average of 6 readings

3.3 The Effect of Segregation on Toughness and Hardness

Table 5 lists the unnotched Charpy impact strength and Rockwell hardness of the impact specimens which were made from 15 and 75 mm casting bars of each alloy in the as-cast, austempered at 350 °C for 5 h and at 400 °C for 50 min conditions. Figures 11 and 12 illustrate the variation of impact strength and hardness of 15 mm and 75 mm specimens in these three conditions for the Ni, Cu, Mn, and Mo ductile irons.

For the as-cast specimens (Fig. 12a), the hardness for all 15 mm specimens is higher than that of 75 mm specimens. There is no significant difference in impact energy for all 15 and 75 mm specimens (Fig. 11a), except the 75 mm Cu alloy has a lower impact value. The hardnesses for all alloys after austempering at 350 °C are slightly greater than for austempering at 400 °C. For the same austempering conditions, there is no significant variance in hardness of each alloy in different diameters. However, the impact values of 15 mm specimens are significantly higher than those of 75 mm specimens. For austempering at 400 °C (Fig. 11c), the impact value of Ni, Cu, and Mn alloys of 15 mm specimens is approximately 15 kg-m, and the impact value of 75 mm specimens is 10 kg-m. The impact value of the Mo alloys is lower, 12 kg-m, and that of 75 mm specimens is 6 kg-m. For austempering at 350 °C (see Fig. 11b), there is no significant difference in impact values of Ni, Cu, and Mn alloys in 15 and 75 mm specimens, whereas that for specimens of Mo alloy stays low.

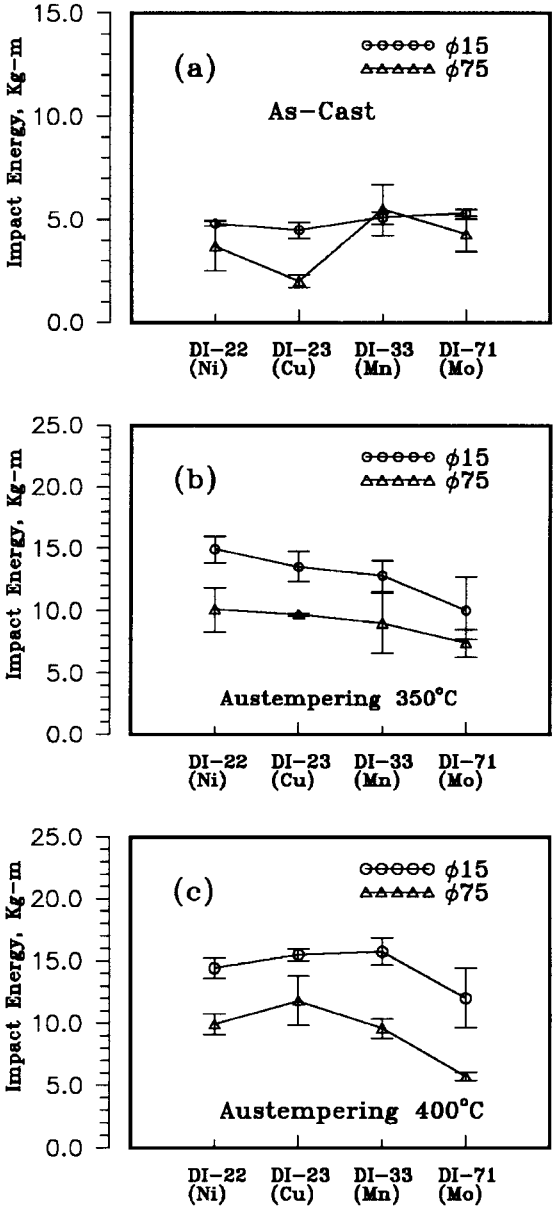

Fig. 11 The impact strength of 15 mm and 75 mm specimens. (a) As-cast condition. (b) After austempering 5 h at 350 °C. (c) After austempering 50 min at 400 °C

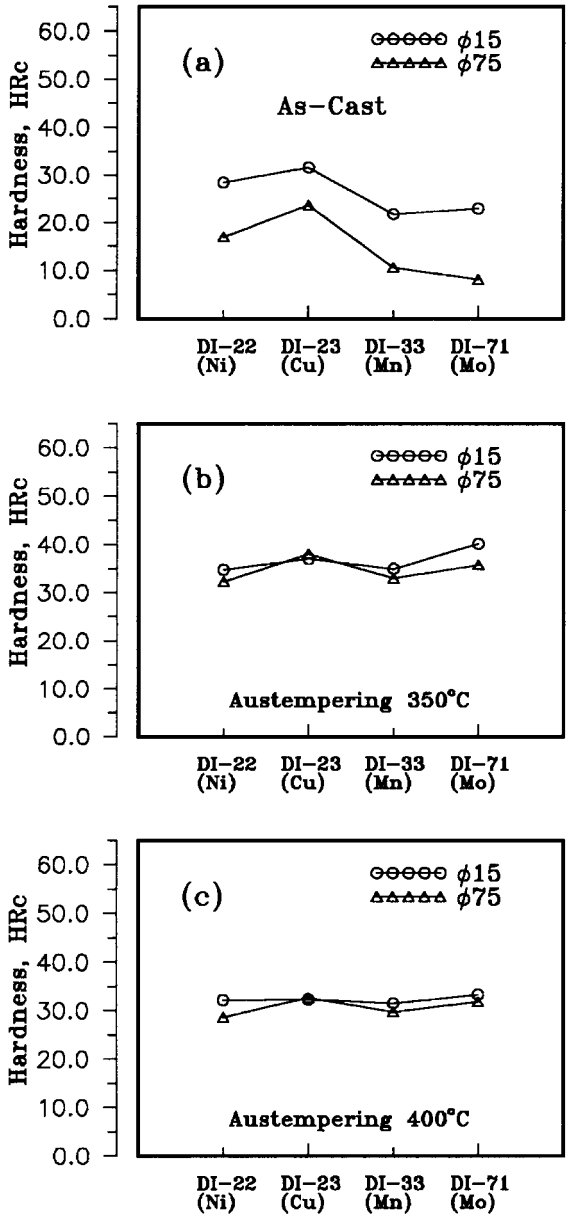

Fig. 12 The Rockwell hardness of 15 mm and 75 mm specimens. (a) As-cast condition. (b) After austempering 5 h at 350 °C. (c) After austempering 50 min at 400 °C

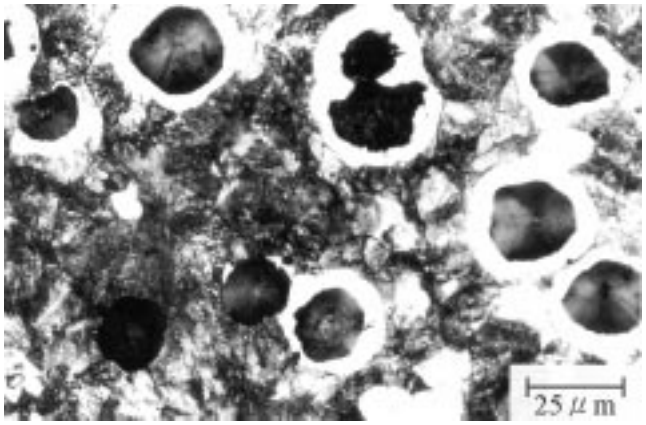

(a)

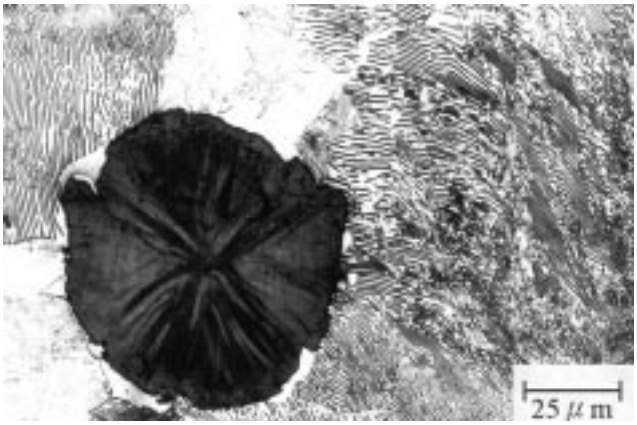

(b)

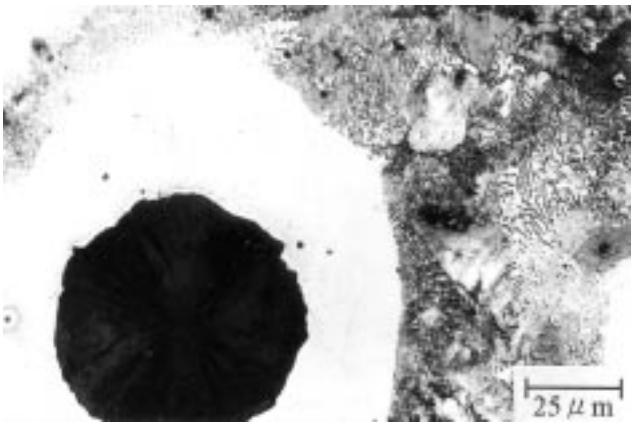

(c)

Fig. 13 Microstructure of as-cast specimens. (a) Ni alloy, 15 mm. (b) Cu alloy, 75 mm. (c) Mn alloy, 75 mm

3.4 Microstructure of Impact Specimens

The as-cast specimens of all 15 mm alloys should have a more rapid cooling rate during solid transformation, so the microstructure of these specimens showed extensive pearlite, as illustrated by the micrograph of the Ni alloy in Fig. 13(a). As for as-cast 75 mm specimens, the ferrite-pearlite ratio is affected by the alloying elements. The ability of Cu to hinder carbon diffusion at the graphite-austenite interface during the eutectoid transformation results in all pearlite being present (Fig. 13b).

Other alloys exhibit substantial ferrite in the as-cast structure with pearlite relegated to near the intercellular regions as the microstructure of Mn alloy in Fig. 13(c) illustrates. The hardness of all as-cast 15 mm specimens alloys is higher than in 75 mm specimens (Fig. 12a), and the Cu-alloyed iron in 75 mm size has the highest hardness and the lowest impact strength among all alloys of the same diameter (see Fig. 11a and 12a).

The microstructures of alloys austempered at 400 °C for 50 min reveal a typical upper bainite structure with plate bainite ferrite and carbon-rich austenite (Fig. 14). In most aspects, the microstructure of Ni, Cu, and Mn alloys is relatively homogeneous throughout the specimens and similar to the micrograph of the Cu alloy shown in Fig. 14(a) and (b). As for the microstructure of the Mo alloy, it is observed that light etching areas stand out in the intercellular regions illustrating the existence of untransformed austenite, which also is associated with microshrinkage porosity (see arrows) as shown in Fig. 14(c) and (d). There are more untransformed areas in 75 mm specimens than in 15 mm specimens. The microstructures of specimens austempered at 350 °C for 5 h show a structure with acicular bainitic ferrite and carbon-rich austenite. Also the Ni, Cu, and Mn alloys completed the first stage bainite reaction, as the micrographs of the Mn alloy show in Fig. 15(a) and (b). The structures of the Mo alloy in the 15 mm and 75 mm specimens also contain the untransformed areas associated with microshrinkage porosity in the intercellular regions (see arrows, Fig. 15c and d); however, only a few unetched areas are found when compared with Fig. 14(c) and (d).

In Fig. 14, 15, and 11, the microstructures of Ni, Cu, and Mn alloys in each austempered condition show completion of the first stage of bainite reaction, and the impact values of these three alloys in the same diameter are not significantly different. Mo has the most extreme segregating tendency of all alloying elements in this study, and it retards the bainite reaction and causes microshrinkage porosity in the intercellular regions. Consequently, the Mo-alloyed irons austempered at 350 and 400 °C have the lowest impact strength among all alloys (see Fig. 11b and c).

4. Conclusions

- The degree of segregation of alloying elements increases with an increase in the diameter of casting bars (i.e., segregation becomes significant as the solidification time of casting increases). The segregation ratio of each element is proportional to the casting modulus.
- Segregation is found with those positive segregating elements, Mn and Mo, and those negative segregating elements, Si, Cu, and Ni. The segregation of Mo is more significant than Mn. The segregation of Cu is more than Ni, and that of Ni is more than Si.
- The austempering temperature is a critical factor affecting the processing window, which is relatively narrow for austempering of 400 °C but wider at 350 °C.
- The microsegregation of alloying elements leads to a reduction in the processing window. The greater the degree of segregation, the less will be the span of the processing window. Due to this ratio, the difficulty of controlling the process of austempering of ductile irons is increased.

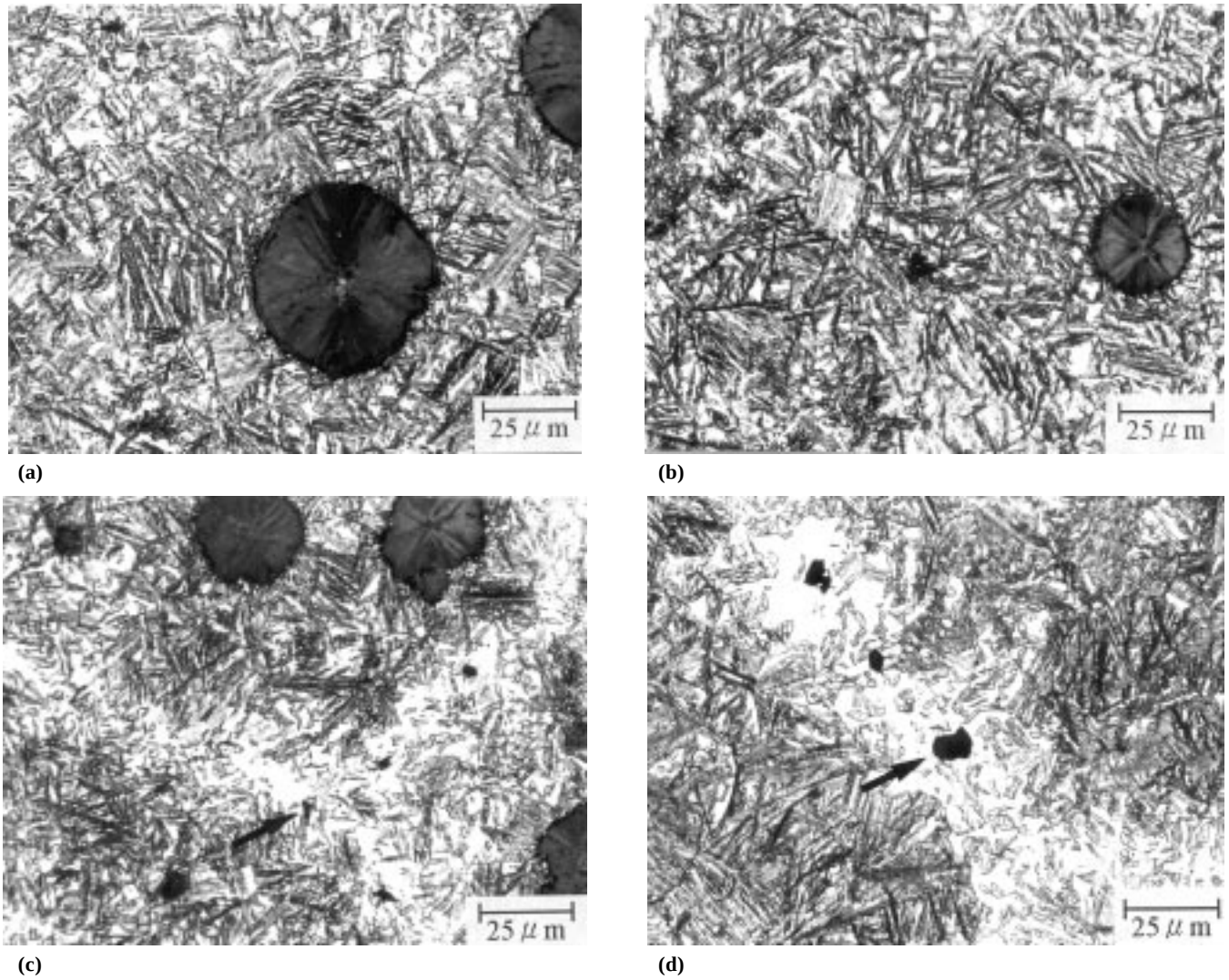

Fig. 14 Microstructure of ADI specimens, austempered at 400 °C for 50 min. The arrows indicate microshrinkage porosity. (a) Cu alloy, 15 mm. (b) Cu alloy, 75 mm. (c) Mo alloy, 15 mm. (d) Mo alloy, 75 mm

- Impact toughness is significantly affected by the segregation, but there is little effect on the hardness. The impact strength for the specimens with less segregation is greater than for those with greater segregation.
- Given the proper austempering treatment, the Ni, Cu, and Mn alloyed irons had approximately the same impact strength. The Mo-alloyed iron had a lower impact strength. This may be attributable to the regions of untransformed austenite in the intercelluar regions, but this may be due to the microporosity present in the Mo-alloyed iron.

Acknowledgments

The authors would like to thank Professor Charlie R. Brooks for reading and commenting on this paper. They also are grateful for the partial financial support of this work by the National Science Council of the R.O.C. under grant No. NSC 80-0405-E011-08 and NSC-82-0405-E011-027.

References

1. P.A. Blackmore and R.A. Harding, The Effect of Metallurgical Process Variables on the Properties of Austempered Ductile Iron, *J. Heat Treating*, Vol 3, 1984, p 310-325
2. J.F. Janowark and R.B. Gundlach, Development of Ductile Iron for Commercial Austempering, *AFS Trans.*, Vol 91, 1983, p 377-388
3. R.C. Voigt, Microstructural Analysis of Austempered Ductile Cast Iron Using the Scanning Electron Microscope, *AFS Trans.*, Vol 91, 1983, p 377-388
4. M. Jonansson, Austenitic-Bainitic Ductile Iron, *AFS Trans.*, Vol 95, 1977, p 117-122
5. D.J. Moore, T.N. Rouns, and K.B. Rundman, The Effect of Heat Treatment, Mechanical Deformation and Alloying Element Additions on the Rate of Bainite Formation in Austempered Ductile Iron, *J. Heat Treating*, Vol 4, 1985, p 7-24
6. D.J. Moore, T.N. Rouns, and K.B. Rundman, Structure and Mechanical Properties of Austempered Ductile Iron, *AFS Trans.*, Vol 93, 1985, p 705-718
7. D.J. Moore, B.S. Shugart, K.L. Hayrynen, and K.B. Rundman, A Microstructure Determination of Isothermal Transformation Diagram in a Low-Alloy Ductile Iron, *AFS Trans.*, Vol 98, 1990, p 519-526

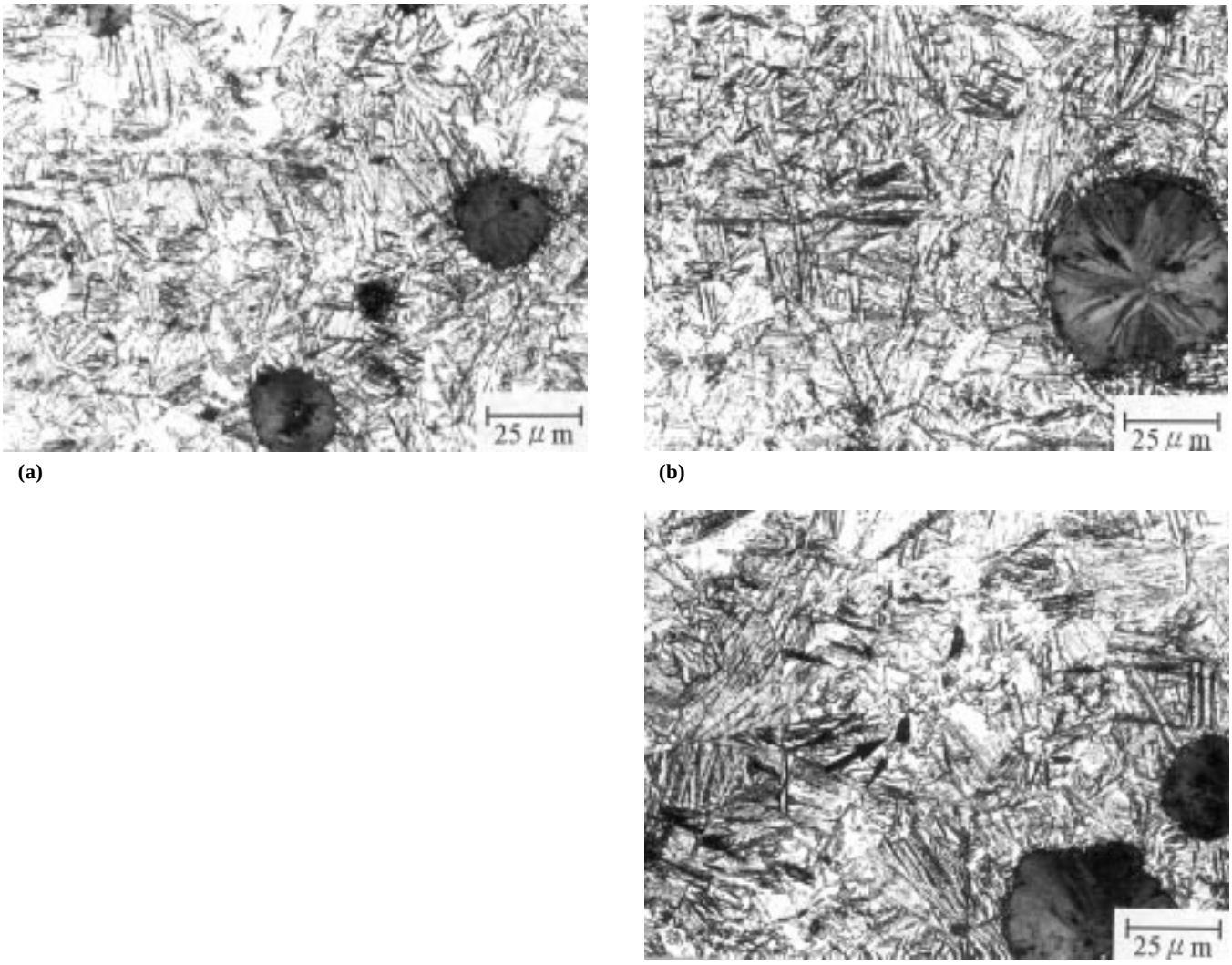

(a) **(b)** **(c)** **(d)**

Fig. 15 Microstructure of ADI specimens, austempered at 350 °C for 5 h. The arrows indicate microshrinkage porosity. (a) Mn alloy, 15 mm. (b) Mn alloy, 75 mm. (c) Mo alloy, 15 mm. (d) Mo alloy, 75 mm

8. D.J. Moore, G.P. Faubert, E.D. McCarty, D.J. Ellerbrock, and K.B. Rundman, Isothermal Transformation Diagram in a Heavy-Section, High-Alloy Ductile Cast Iron, *AFS Trans.*, Vol 98, 1990, p 49-457
9. K. Yasue, T. Nisio, Y. Yamada, and Y. Obata, Effects of Alloying Elements and Austenitizing Conditions on the Isothermal Transformation Diagram of Ductile Cast Iron, *Imono*, Vol 63, 1991, p 595-600
10. J.P. Chobaut, P. Brenot, and J. M. Schissler, Secondary Martensite Formation During the Tempering of Bainite S. G. Cast Iron., *AFS Trans.*, Vol 96, 1988, p 475-480
11. K.B. Rundman and R.C. Klug, An X-ray and Metallographic Study of an Austempered Ductile Iron, *AFS Trans.*, Vol 90, 1982, p 499-508
12. B.Y. Lin, A Study on Austemperability of Ductile Iron, Master Thesis, 1987, *NTIT*, R.O.C.
13. Y.J. Park, R.B. Gundlach, and J.F. Janowark, Monitoring the Bainite Reaction during Austempering of Ductile Steel by Resistivity Measurement, *AFS Trans.*, Vol 95, 1987, p 411-416
14. B.Y. Lin, E.T. Chen, and T.S. Lei, The Use of Electrical Conductivity on the Study of the Austemperability of Ductile Irons, NSC 80-0405-E011-08, R.O.C.
15. D.J. Moore, T.N. Rouns, and K.B. Rundman, Effect of Manganese on Structure and Properties of Austempered Ductile Iron: A Processing Window Concept, *AFS Trans.*, Vol 94, 1986, p 255-264
16. N. Darwish and R. Elliott, Austempering of Low Manganese Ductile Irons—Part 1: Processing Window, *Materials Science and Technology*, Vol 9, 1993, p 572-585
17. R.C. Voigt and C.R. Loper, Jr., Austempered Ductile Iron—Process Control and Quality Assurance, *J. Heat Treating*, Vol 3, 1984, p 291-309
18. B.V. Kovacs, Austempered Ductile Iron: Fact and Fiction, *Modern Casting*, March 1990, p 38-41
19. G. Jolley, Segregation During Solidification of Nodular Cast Iron, *The Solidification of Metals, London, Iron and Steel Inst.*, Vol 110, 1968, p 242-250
20. N.K. Datta and N.N. Engel, Electron Microprobe Study of the Distribution of Si, Cu, Ni, Mn, Mo, and Cr in Ductile Iron, *AFS Trans.*, Vol 84, 1976, p 431-436
21. P.C. Liu and C.R. Loper, Jr., Electron Microprobe Study of the Intercellular Compounds in Heavy Section Ductile Iron, *AFS Trans.*, Vol 89, 1981, p 131-140

22. R. Boeri and F. Weinberg, Microsegregation in Ductile Iron, *AFS Trans.*, Vol 97, 1989, p 179-184

23. J.M. Schissler and J. Saverna, The Effect of Segregation on the Formation of Austempered Ductile Iron, *J. Heat Treating*, Vol 4, 1985, p 167-176

24. K.L. Hayrynen, G.P Faubert, D.J. Moore, and K.B. Rundman, Heavy Section ADI: Microsegregation, Microstructure, and Tensile Properties, *AFS Trans.*, Vol 97, 1989, p 747-756

25. G.P Faubert, D.J. Moore, and K.B. Rundman, Heavy Section ADI: Tensile Properties in the As-Cast and Austempered Condition, *AFS Trans.*, Vol 99, 1991, p 551-561

26. M.C. Flemings, Solidification Processing, McGraw-Hill, New York, 1974, p 11

27. B.Y. Lin, The Effect of Alloy Elements on the Austemper-Transformation of Ductile Irons, Ph.D. Thesis, 1995, *NTIT*, R.O.C.